# Impact of Fundamental Temperature Fluctuations on the Frequency Stability of Metallo-Dielectric Nanolasers

Sizhu Jiang<sup>®</sup>, Si Hui Pan<sup>®</sup>, Suruj S. Deka, Cheng-Yi Fang<sup>®</sup>, Zijun Chen, Yeshaiahu Fainman, *Fellow, IEEE*, and Abdelkrim El Amili

Abstract—The capability of nanolasers to generate coherent light in small volume resonators has made them attractive to be implemented in future ultra-compact photonic integrated circuits. However, compared to conventional lasers, nanolasers are also known for their broader spectral linewidths, that are usually on the order of 1 nm. While it is well known that the broad linewidths in light emitters originate from various noise sources, there has been no rigorous study on evaluating the origins of the linewidth broadening for nanolasers to date to the best of our knowledge. In this manuscript, we investigate the impact of fundamental thermal fluctuations on the nanolaser linewidth. We show that such thermal fluctuations are one of the intrinsic noise sources in a sub-wavelength metal-clad nanolaser inducing significant linewidth broadening. We further show that with the reduction of the nanolaser's dimensions, i.e., mode volume, and the increase of the ambient temperature, such linewidth broadening is enhanced, due to the effect of more pronounced fundamental thermal fluctuation. Specifically, we show that the finite linewidths induced by the thermal fluctuations at room temperature are 1.14nm and 0.16nm, for nanolasers with core radii of 250nm and 750nm, respectively. Although our study was performed on a metallo-dielectric nanolaser, it is reasonable to assume that, in general, other nanolaser architectures are also more prone to thermal fluctuations, and hence exhibit larger finite linewidths than conventional large mode volume lasers.

Index Terms—Semiconductor nanolasers, fundamental thermal fluctuations, thermal noise, Langevin method, nanolaser linewidth.

Manuscript received May 6, 2019; revised July 16, 2019; accepted August 5, 2019. Date of publication August 21, 2019; date of current version September 4, 2019. This work was supported in part by the Defense Advanced research Projects Agency (DARPA) and DARPA Nascent Light-Matter Interactions (NLM), in part by the Office of Naval Research (ONR) Multidisciplinary University Research Initiative (MURI), in part by the National Science Foundation (NSF) under Grant DMR-1707641, Grant CBET-1704085, Grant ECCS-1405234, Grant ECCS-1644647, Grant CCF-1640227, and Grant ECCS-1507146, in part by the NSF Engineering Research Center (ERC) for Integrated Access Networks (CIAN), in part by the Semiconductor Research Corporation (SRC), and in part by the Cymer Corporation. (Corresponding author: Abdelkrim El Amili.)

- S. Jiang, S. S. Deka, Z. Chen, Y. Fainman, and A. El Amili are with the Department of Electrical and Computer Engineering, University of California at San Diego, San Diego, CA 92093-0407 USA (e-mail: sij023@ucsd.edu; sdeka@ucsd.edu; zic005@ucsd.edu; faiman@eng.ucsd.edu; aelamili@eng.ucsd.edu).
- S. H. Pan is with the Department of Physics, University of California at San Diego, San Diego, CA 92093-0407 USA (e-mail: h0pan@ucsd.edu).
- C.-Y. Fang is with the Materials Science and Engineering Program, University of California at San Diego, San Diego, CA 92093-0407 USA (e-mail: c5fang@eng.ucsd.edu).

Color versions of one or more of the figures in this article are available online at http://ieeexplore.ieee.org.

Digital Object Identifier 10.1109/JQE.2019.2936592

#### I. Introduction

THE miniaturization of optical resonators has established **I** nanolasers as promising coherent light source candidates for future integrated nanophotonics with wide applications in bio-sensing [1]-[3], imaging [4]-[6], far-field beam synthesis [7] and optical interconnects [8]. The ultra-compact mode volume of nanolasers also enables them to exploit the cavity quantum electrodynamics (OED) effect [9]-[12]. In these nanocavities, conspicuous Purcell enhancement helps to dramatically increase the modulation speed and lower the power consumption for optical communication systems. However, shrinking the dimension of a nanolaser can also be detrimental to its performance. One of the intrinsic issues with nanoscale resonators is that, fundamental thermal fluctuation (FTF) is expected to be more pronounced in comparison to conventional lasers. According to the fluctuation-dissipation theorem, the variance of the temperature fluctuation  $\Delta T$  is inversely proportional to the optical mode volume V [13], [14]:

$$\langle \Delta T^2 \rangle = \frac{k_B T^2}{\rho c V} \tag{1}$$

where T is the classical temperature,  $\rho$  is the density of the host material  $(g \cdot cm^{-3})$ , c is the specific heat capacity  $(J/g \cdot$ K), and  $k_B$  is the Boltzmann constant (J/K). In semiconductor lasers, this continuous thermal fluctuation perturbs the refractive index of the resonator through the thermo-refractive effect, and hence causes the resonance frequency to fluctuate around its mean. As shown in (1), the thermal noise increases with decreasing mode volume and increasing temperature. Consequently, the bigger noise will impose a more prominent limitation on the frequency stability of the nanoscale light emitters. Therefore, understanding the impact of FTF on a nanolaser's spectral linewidth is of crucial importance, since FTF can be one of the dominant contributions to the broad linewidths measured in various nanolasers, that are usually on the order of 1nm [15]-[27]. Evaluating the linewidth broadening caused by FTF in nanolasers would be the first step towards engineering nanolasers to be employed in applications where narrow linewidth is desired, such as coherent optical communication [28] and near-field spectroscopy [29].

In this manuscript, we theoretically study the impact of FTF on the spectral properties of metallo-dielectric nanolasers in terms of their frequency noise and linewidth broadening. We first introduce the nanolaser architecture to be analyzed in Section II. Details for calculating the spectral properties of a

nanolaser are also presented here. In Section III, to elucidate the effect of a nanolaser's dimension, we evaluate and compare the frequency noise and linewidth broadening generated by FTF in two nanolasers with different radii. The temperature-dependent linewidth broadening is also presented and analyzed. In Section IV, we further consider how the geometry of a nanolaser would alters its linewidth broadening induced by FTF. Comparison between the simulation result and empirical results reported in previous studies is also discussed. Finally, summary and conclusions of FTF's effect on a nanolaser's spectral performance are presented in Section V.

#### II. THEORETICAL MODEL

In semiconductor resonators, thermal fluctuations perturb the refractive index of the constituent materials. Therefore, the temperature fluctuation  $\Delta T(\vec{r},t)$  lead to a fundamental uncertainty of the cavity resonance via the thermo-refractive effect. By solving the temperature-perturbed wave-equation, the transient fluctuation of the frequency resonance  $\Delta v(t)$  with respect to the center resonance frequency  $v_0$  can be expressed as [30]:

$$\Delta v(t) = -\frac{v_0}{n} \frac{dn}{dT} \Delta \bar{T}(t)$$

$$= -\frac{v_0}{n} \frac{dn}{dT} \int_V \Delta T(\vec{r}, t) |E(\vec{r})|^2 d\vec{r}$$
(2)

where  $\Delta \bar{T}(t)$  is the average thermal fluctuation over the mode volume,  $\vec{E}(\vec{r})$  is the normalized electric field distribution of the eigenmode, n is the refractive index of the gain material, and dn/dT is the thermo-optic coefficient. The center frequency  $v_0$  can be determined by various approaches [31], [32]. In this work,  $v_0$  is found by performing a three-dimensional (3-D) finite-element-method (FEM) simulation in COMSOL Multiphysics. The lasing mode is expected to have the highest quality factor and the lowest lasing threshold among the eigenmodes that lie within the gain spectrum of InGaAsP [33]. As shown in (2), the linewidth broadening can be estimated by determining  $\Delta T(\vec{r},t)$  and  $E(\vec{r})$ . Hence, in the following section, we first solve the electric field distribution  $E(\vec{r})$  within the resonator. Then, we present the theoretical approach adopted to quantify the thermal fluctuations  $\Delta T(\vec{r},t)$ .

#### A. Metallo-Dielectric Nanolaser Architecture

The architecture of the metallo-dielectric nanolaser under consideration throughout the manuscript is depicted in Fig. 1(a). The nanolaser has an InGaAsP gain medium with a radius of  $R_I$  and a height of H. The gain region is wrapped by a SiO<sub>2</sub> shield, whose thickness is optimized to lower the lasing threshold [34]. The total radius of the InGaAsP core plus the SiO<sub>2</sub> shield is labelled as  $R_2$ . The values of  $R_I$ ,  $R_2$  and H for the devices N-250 and N-750 under consideration are given in Table. I. A thick Ag cladding that covers the dielectric shield not only allows high mode confinement ( $\Gamma \sim 86\%$ ), but also facilitates the heat dissipation of the nanolaser [15], [16], [20], [22], [35]. The metallo-dielectric nano-resonators are designed to support a transverse electric (TE) mode.

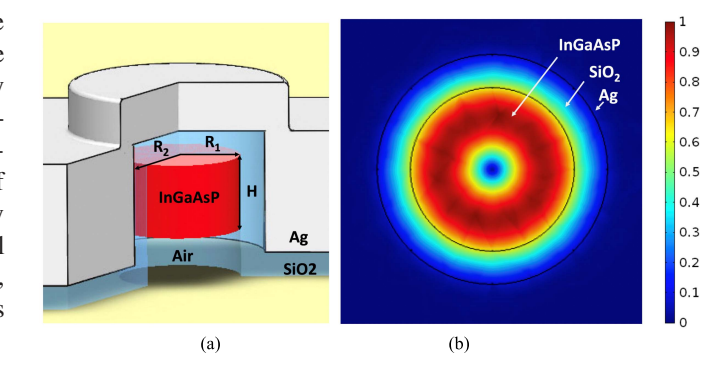


Fig. 1. (a) 3D schematic of the metallo-dielectric nanolaser.  $R_1$  is the radius of the gain medium InGaAsP,  $R_2$  is the total radius of InGaAsP plus SiO<sub>2</sub> dielectric shield, and H is the height of the InGaAsP. The pillar is covered by adequately thick Ag cladding. The values are given in Table.I. (b) Normalized electric field distribution profile of the cross section (chosen at the center of the gain medium InGaAsP) of N-250 obtained from 3D FEM simulation. The black circles are the interfaces of InGaAsP/SiO<sub>2</sub> and SiO<sub>2</sub>/Ag, respectively. Effective confinement in the gain region can be observed.

 $\label{thm:constraint} \textbf{TABLE} \ \textbf{I}$  Dimension Parameters of the Nanolasers for Calculation

Parameter (unit)	N-250	N-750
R <sub>1</sub> (nm)	250	750
$R_2(nm)$	350	900
H (nm)	300	300

For example, N-250 supports a first order  $TE_{011}$  mode, as shown in Fig. 1(b).

To obtain the continuous electric field  $E(\vec{r})$  of a nanolaser shown in (2), a 3-D FEM simulation in COMSOL is first performed to extract the discrete electric field distribution. These discrete data are then fitted into continuous analytical solutions, that are Bessel functions, due to the radial symmetry of the cylindrical metallo-dielectric nanolasers. For example, the electric field solutions of the  $TE_{011}$  mode of N-250, as shown in Fig. 1(b), are the first order Bessel functions, that can be expressed as:

$$E_{1,2}(r) = A_{1,2}J_1(k_{1,2}r) + B_{1,2}Y_1(k_{1,2}r), \quad 0 \le r \le R_2$$
  

$$E_3(r) = A_3I_1(k_3r) + B_3K_1(k_3r), \quad r \ge R_2$$
(3)

where the subscripts denote different regions, with 1 being InGaAsP, 2 being SiO<sub>2</sub> and 3 being Ag. Fig. 2 presents the plotting of (3) based on the discrete FEM simulation data. Approaches other than FEM simulations, such as in [36], can also be applied to derive the electric field in the semiconductor regions.

Next, we derive the thermal fluctuations solutions  $\Delta T (\vec{r}, t)$ , the other prerequisite for evaluating the frequency shift  $\Delta v (t)$ .

# B. Calculations of the Fundamental Thermal Noise Using Langevin Approach

To calculate the thermal fluctuations,  $\Delta T(\vec{r}, t)$ , a 2-D heat transport model with the boundary conditions imposed by the nanocavity structure is adopted. This model is based on

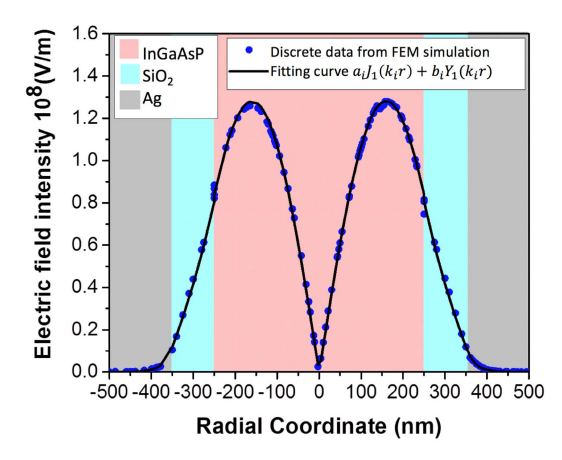


Fig. 2. Transverse electric field distribution of the metallo-dielectric nanolaser N-250. Radius of the gain region:  $R_1 = 250$ nm; outer radius  $R_2 = 350$ nm. Radial coordinates greater than 350nm represent the metal cladding region. Blue dots are the discrete value obtained from numerical simulation. Solid black line is the corresponding fitting curve.

a general assumption that the thermal fluctuations can be decomposed into a radial mode and a longitudinal mode. For metallo-dielectric nanolasers, the in-plane radial mode will be chosen for the following calculation. This choice is validated by two facts: 1) the in-plane-mode-dominated heat dissipation; 2) the resonant frequency of the TE mode shows more dependence on radial properties of the resonator. The 2-D heat transport model that we intend to use is governed by the stochastic heat transport equation. This equation includes a *Langevin* noise source  $F(\vec{r}, t)$  to account for the randomness of the thermal fluctuation [37], [38], and is expressed as:

$$\frac{\partial \Delta T(\vec{r},t)}{\partial t} - D_T \nabla_{\vec{r}}^2 \Delta T(\vec{r},t) = F(\vec{r},t)$$
 (4)

where  $D_T(cm^2s^2)$  is the thermal diffusion constant that we assume is homogeneous throughout each medium.  $D_T = \eta/\rho c$ , in which  $\eta(W/cm \cdot K)$  is the thermal conductivity. Because the driving source  $F(\vec{r},t)$  is uncorrelated in space and time, the Green's function method is applied to derive the analytical solution for the thermal fluctuations  $\Delta T(\vec{r},t)$  [38]. To compute the broadening of the emission linewidth, the power spectral density (PSD) of the frequency noise  $S_f(w)$  needs to be evaluated (where the subscript denotes the frequency noise). We restrict the noise source considered in this manuscript to only FTF. Therefore, the frequency noise is solely generated by thermal noise, and hence knowing  $S_f(w)$  requires knowledge of the PSD of the thermal noise  $S_{\Delta T}(w)$ . A Fourier transform is performed on the corresponding Green's function of (4) and gives:

$$iwG(\vec{r}, \vec{r}'; iw) - D_T \nabla_{\vec{r}}^2 G(\vec{r}, \vec{r}'; iw) = \delta(\vec{r} - \vec{r}')$$
 (5)

where w is the Fourier angular frequency and r is the coordinate of the spatially uncorrelated Langevin heat source. The thermal fluctuations in the frequency domain then can be derived from the definition of Green's function as:

$$\Delta \tilde{T}(\vec{r}, w) = \int_{V} G(\vec{r}, \vec{r}'; iw) \tilde{F}(\vec{r}, iw) d\vec{r}'$$
 (6)

Equation (6) shows that, in order to obtain  $S_{\Delta T}(w)$  to evaluate the parasitic frequency noise  $S_f(w)$ , the spectral density of the *Langevin* noise source  $F(\vec{r},t)$  is needed. The spectral autocorrelation of the *Langevin* source that satisfies the fluctuation-dissipation theorem is shown to be [39], [40]:

$$\langle \tilde{F}(r, iw) \, \tilde{F}^*(r', iw') \rangle = \frac{4\pi \, D_T \, Ak_B T^2}{\rho \, c \, V} \nabla_r \nabla_{r'} \delta \left( r - r' \right) \delta \left( w - w' \right) \quad (7)$$

where A is the area of the InGaAsP cross-section. Here we assume that the heat source lies in the gain medium, since most of the energy is well confined to it (see Fig. 1(b)). According to Wiener-Kintchin theorem, the single-sided PSD  $S_{\Delta T}(w)$  is shown to be (see Appendix. B):

$$S_{\Delta T}(w) = \frac{1}{\pi} \langle \Delta \tilde{T}(w) \Delta \tilde{T}^*(w') \rangle = \frac{4Ak_B T^2}{\rho c V} \times \int_{V} \int_{V} Re \left[ G(r, r'; iw) \right] |E(r)|^2 |E(r')|^2 r r' dr dr'$$
(8)

The vanishing of the space-dependence of  $S_{\Delta T}(w)$  is due to the fact that spatially-dependent thermal fluctuations are integrated over the entire mode volume, as shown in (2).

To obtain the particular solutions  $G\left(r,r';iw\right)$  in (8) for each domain, appropriate boundary conditions are applied to the general solutions. Due to the axial symmetry of the nanolasers, the general solutions are Bessel functions of the zeroth order. The Ag cladding acts as an effective heat sink. Therefore, we assume that fluctuations are absent at the SiO<sub>2</sub>/Ag interface, i.e.,  $\Delta T \mid_{R_2} = 0$ . With the detailed boundary conditions shown in Appendix B, we arrive at the Green's function solutions for different regions as:

$$0 \leq r \leq r',$$

$$G_{1}^{<}(r, r'; iw) = g_{1}(r') J_{0}(k_{\rho 1}r)$$

$$r' \leq r \leq R_{1},$$

$$G_{1}^{>}(r, r'; iw) = g_{2}(r') J_{0}(k_{\rho 1}r) + h_{2}(r') H_{0}^{(1)}(k_{\rho 1}r)$$

$$R_{1} \leq r \leq R_{2},$$

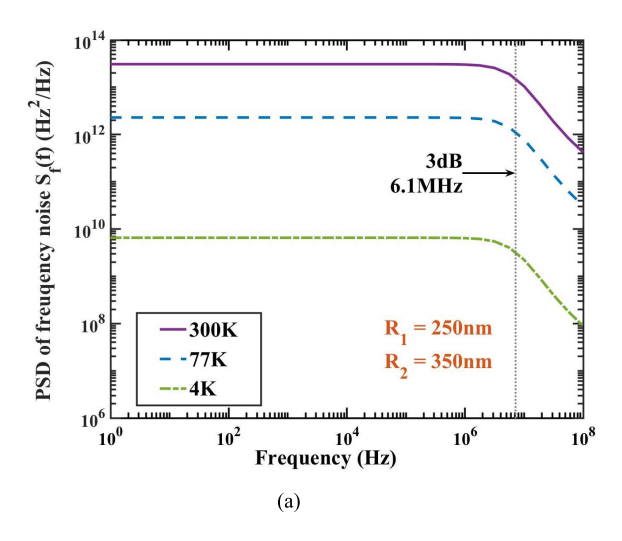
$$G_{2}(r, r'; iw) = g_{3}(r') J_{0}(k_{\rho 2}r) + h_{3}(r') Y_{0}(k_{\rho 2}r)$$
(

where  $k_{\rho 1} = \sqrt{-iw/D_1}$ ,  $k_{\rho 2} = \sqrt{-iw/D_2}$ . The Hankel Function  $H_0^{(1)}$  accounts for the decaying of the heat diffusion away from the heat source and satisfies the singularity at the point heat source [41]. The expressions for  $g_i$  and  $h_i$  are given in Appendix. C. Our analytical solutions present the first set of solutions of the thermal fluctuations in composite structures with semiconductor gain and metal clad.

By substituting the solutions for the Green's function and the electric field as stated in (9) and (3) into (8), we can obtain the PSD for FTF  $S_{\Delta T}(w)$ . Subsequently, the frequency noise  $S_f(w)$  introduced by FTF and the linewidth broadening will be calculated next.

## C. Frequency Noise and Linewidth Broadening

To evaluate the PSD of the frequency noise generated by FTF, a Fourier transform is performed on the transient



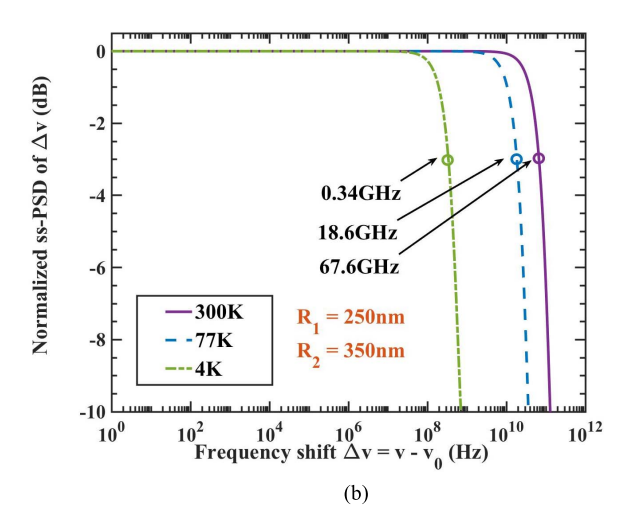


Fig. 3. (a) PSD of the frequency noise  $S_f(f)$  due to FTF at different ambient temperatures 300K (purple solid line), 77K (blue dashed line), and 4K (green dash-dotted line) in N-250. The grey vertical dotted lines are the 3-dB cut-off frequency. (b) The normalized single-sided PSD  $S_{dv}(\Delta v)$  of the frequency shift to the central frequency  $\Delta v = v - v_0$  (Hz) due to FTF under different ambient temperatures 300K, 77K, and 4K for N-250. The 3-dB are 67.6GHz, 18.6GHz, and 0.34GHz, that correspond to linewidth broadenings of 1.14nm, 0.31nm, and 5.4pm under 300K, 77K, and 4K, respectively.

autocorrelation of the instantaneous frequency deviation  $\Delta v(t)$  in (2). Since  $\Delta v(t) = \Delta w(t)/2\pi$ , we can also relate  $S_f(f)$  and  $S_f(w)$  as:

$$S_f(w) = 4\pi^2 S_f(f) = 4\pi^2 \left(-\frac{v_0}{n} \frac{dn}{dT}\right)^2 S_{\Delta T}(w)$$
 (10)

where  $f = w/2\pi$  is the Fourier Transform basis frequency. To evaluate the linewidth broadening, we transfer the frequency noise into the statistics of the phase noise. The variance of the fluctuation of the optical phase  $\Delta \phi$  reads [42]:

$$\langle \Delta \phi^2 \rangle = \frac{\tau^2}{\pi} \int_0^{+\infty} S_f(w) \frac{\sin^2\left(\frac{w\tau}{2}\right)}{\left(w\tau/2\right)^2} dw \tag{11}$$

where  $\tau$  is the delay time in the autocorrelation function of the electric field, that is defined by:

$$\langle E(t) E^*(t-\tau) \rangle = I_0 \exp(j2\pi v_0 \tau) \langle \exp(j\Delta\phi) \rangle$$
 (12)

in which  $\langle exp\left(j\,\Delta\phi\right)\rangle = exp\left(-\langle\Delta\phi^2\rangle/2\right)$  by assuming that  $\Delta\phi$  follows a Gaussian distribution. This can be justified by the fact that the phase noise is introduced by many independent noise events [43]. We assume that FTF is the only noise source in the nanocavity, and the finite linewidth  $\Delta v$  is solely generated by the thermal noise, with Schawlow-Townes-Henry linewidth being neglected. As a result, the linewidth broadening can be taken to be twice the 3-dB bandwidth of the single-sided  $S_{\Delta v}\left(\Delta v\right)$  spectrum, which is the spectral decomposition of (12).  $\Delta v = v - v_0$  is the frequency deviation from the center frequency. Then, we can derive  $S_{\Delta v}\left(\Delta v\right)$  by taking a Fourier transform of (12) yielding,

$$S_{\Delta v} (\Delta v) = I_0 \int_{-\infty}^{\infty} \exp(j2\pi \, \Delta v \tau) \exp\left(-\frac{\langle \Delta \phi^2 \rangle}{2}\right) d\tau$$
(13)

In the following section, we present the calculation results of both frequency noise and linewidth broadening using the parameters summarized in Table. II.

TABLE II

MATERIAL PARAMETERS OF THE NANOLASERS FOR CALCULATIONS
OF THE LINEWIDTH AT 300K. [47]

Symbol (unit)	Quantity	InGaAsP	SiO <sub>2</sub>
η (W/cm · K)	Thermal conductivity	4.4	1.0
<i>c</i> (J/g⋅K)	Specific heat capacity	0.31	0.74
$\rho$ (g/cm <sup>3</sup> )	density	4.8	2.2
$D_T  (\mathrm{cm}^2/\mathrm{s})$	Thermal diffusion constant	2.90	0.61
n	Refractive index	3.4	1.46
$dn/dT \ (10^{-4}/\text{K})$	Thermo-optic coefficient	2	0.14

# III. RESULTS

In this section, numerical simulation results of the impact of FTF on the frequency noise and linewidth broadening in N-250 and N-750 are presented. Fig. 3(a) shows the PSD of the frequency noise  $S_f(f)$  of N-250 under ambient temperature 300K, 77K and 4K. The frequency noise  $S_f(f)$  spectra behave as a low pass filter with a 3-dB bandwidth of  $\sim$  6.1MHz. As shown in Fig. 3(a),  $S_f(f)$  at room temperature (300K) is 4 orders of magnitude higher than that at 4K. Utilizing (10) – (13), the normalized single-sided PSD  $S_{\Delta v}(\Delta v)$  for the frequency shift around the center frequency  $\Delta v = v - v_0$ can be calculated and shown in Fig. 3(b). From this figure, the finite linewidth can then be read out as twice the 3-dB bandwidth of  $S_{\Delta v}(\Delta v)$ . We then convert  $\Delta v$  into  $\Delta \lambda$  for a more straight-forward understanding of the results. The linewidth broadening caused by FTF are estimated to be 1.14nm, 0.31nm and 5.4pm at 300K, 77K, and 4K, respectively. As we can see for N-250, due to the ultra-small optical cavity, FTF imposes a large limitation on the resonance stability via the thermorefractive effect and induces a pronounced spectral linewidth under room temperature.

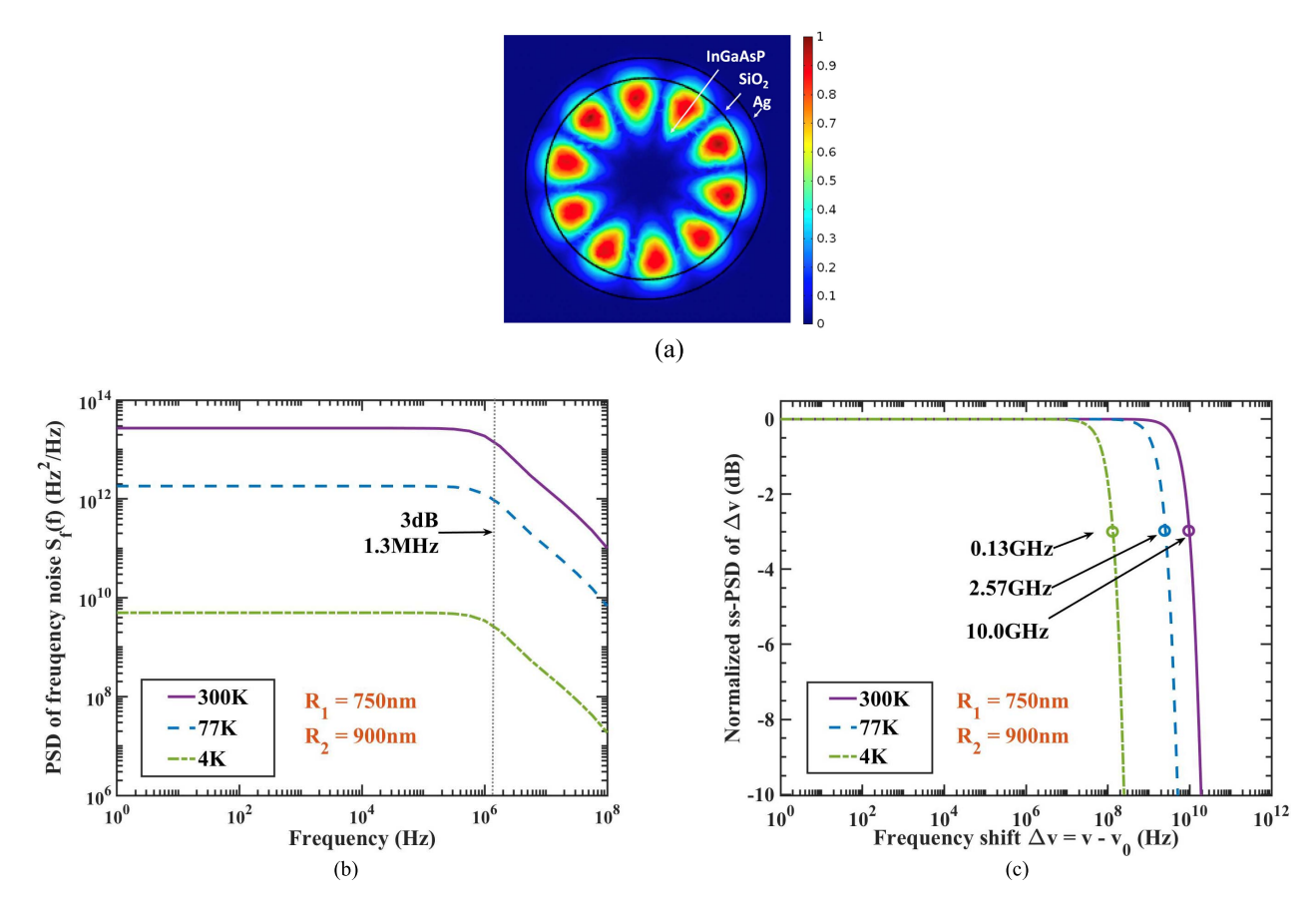


Fig. 4. (a) Normalized electric field distribution profile of the cross section (chosen at the center of the gain medium InGaAsP) of N-750 obtained from 3D FEM simulation. (b) PSD of the frequency noise  $S_f(f)$  due to FTF at different ambient temperatures 300K (purple solid line), 77K (blue dashed line), and 4K (green dash-dotted line) in N-750. The grey vertical dotted lines are the 3-dB cut-off frequency. (c) The normalized single-sided PSD  $S_{\Delta v}$  ( $\Delta v$ ) of the frequency shift to the central frequency  $\Delta v = v - v_0$  (Hz) due to FTF under different ambient temperatures 300K, 77K, and 4K for N-750. The 3-dB are 10.0GHz, 2.57GHz, and 0.13GHz, that correspond to linewidth broadenings of 0.16nm, 0.04nm, and 2pm under 300K, 77K, and 4K, respectively.

To better elucidate the impact of the decreasing mode volume, we investigate and compare the frequency noise and linewidth broadening in a larger cavity N-750 at the same temperatures. While N-250 has an inner radius of  $R_I$  =250nm and an outer radius  $R_2$  = 350nm, N-750 has  $R_I$  =750nm and  $R_2$  = 900nm. The electric field profile of N-750 from 3-D FEM simulation is depicted in Fig. 4(a). As five lobes in a semicircle are shown, the electric field solutions of N-750 are the fifth-order Bessel functions. Same fitting method described in Section II-A is adopted to derive a continuous field distribution from the discrete data obtained from FEM simulations.

The PSD of frequency noise spectra for the device N-750 are presented in Fig. 4(b). To understand how the dimensions of nanoscale cavities influence their linewidth performance, we compare the values at the plateau for N-250 and N-750 at the same temperature. From the observation of these results, a slightly lower frequency noise generated by FTF could be seen for N-750. Moreover, the 3-dB bandwidth of  $S_f(f)$  for N-750, which is around 1.3MHz, is noticeably smaller than that of N-250, which is around 6.1MHz. A comparison between Fig. 3(a) and Fig. 4(b) implies that the nanoscale cavities not only escalate the frequency noise in low frequencies, but also expand the bandwidth for the thermal fluctuations.

Fig. 4(c) shows the linewidth broadening caused by FTF for N-750. We estimate the linewidth broadenings due to FTF as 0.16nm, 0.04nm and 2pm, corresponding to ambient temperatures of 300K, 77K and 4K, respectively. By comparing the values of the two devices for the same temperature, the significantly large difference between N-250 and N-750 in linewidths is observed. This confirms the hypothesis we made in the last section that a larger finite linewidth will be generated due to the reduction of the device dimensions. For instance, at room temperature (300K), N-250 has a radius 3 times smaller than that of N-750 while showing a 7 times larger thermal broadening compared to that of N-750. Our calculation corroborates the idea that nanoscale optical cavities are more prone to FTF than lasers with larger mode volumes, and thus exhibits broader linewidths due to the parasitic frequency noise.

Other than nanolaser's dimension, the ambient temperature is also a crucial factor in determining the finite linewidth generated by FTF. Fig. 5 shows the trend of the linewidth increasing temperature for N-250 and N-750. Discrete ambient temperatures are chosen for revealing the trend, as metal-clad nanolasers are reported to show lasing action under these temperatures [20], [22], [44]–[46]. An almost linear relation between linewidth broadening caused by FTF and ambient

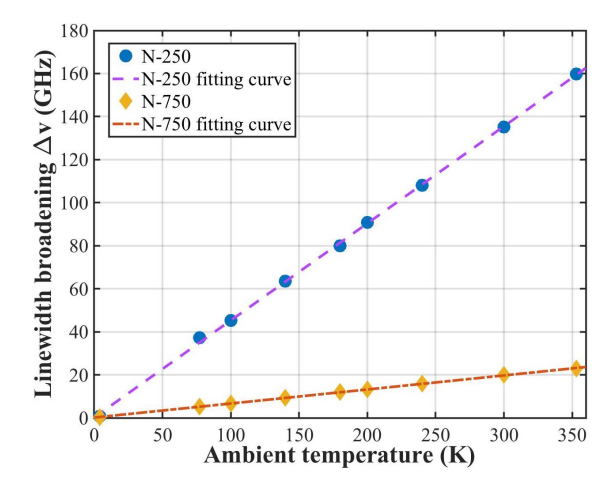


Fig. 5. Linewidth broadening of N-250 and N-750 caused by FTF at ambient temperatures of 4K, 77K, 100K, 140K, 180K, 200K, 240K, 300K, as reported in previous studies, and 353K, as estimated by [47]. For N-250, the fitting curve is  $\Delta v(GHz)$ =0.4511×T(K)+0.1578, with a coefficient of determination  $R^2 = 0.9995$ . For N-750,  $\Delta v(GHz)$ =0.06525×T(K)+0.1488, with  $R^2 = 0.9993$ .

temperature can be seen for both N-250 and N-750. A linear fitting for N-250 shows  $\Delta v(GHz) = 0.4511 \times T(K) + 0.1578$ . Similarly, for N-750 the curve can be fitted into  $\Delta v(GHz) = 0.06525 \times T(K) + 0.1488$ . For the purpose of practical implementation, the fitting curves provide a good estimation for the finite linewidths generated due to FTF at any other temperature.

# IV. DISCUSSION

We further study how the linewidth broadening from thermal fluctuations depends on a nanolaser's geometry, given that the electric field distribution of a nanolaser and the Green's function solutions are both geometry-dependent. We show that given a fixed outer radius  $R_2$ , the linewidth broadening  $\Delta v$  (in Hz) due to FTF also shows a slight dependence on the radius of the active region  $R_1$ . Table. III presents the linewidth broadening under room temperature as  $R_1$  varies around its optimal thickness [34], i.e. lowest lasing threshold. As shown for both  $R_2 = 350nm$  and  $R_2 = 900nm$ , a larger gain radius  $R_1$  induces a smaller finite linewidth  $\Delta v$ . However, the variation of  $\Delta v$  caused by the radius change is only  $\sim 1\%$  of  $\Delta v$ . Therefore, the linewidth broadening shows trivial dependence on the radius of  $R_1$  with a fixed  $R_2$ , on the premise that  $R_1$  varies within its optimal region.

Although the work presented here is based purely on numerical analysis, a comparison with experimental results found in literature can still be made. The N-750 device studied in this work is very similar to a device, whose lasing characterization has already been reported in [20], in terms of both physical dimension and material composition. The only difference is that instead of InGaAsP, InGaAs is utilized as the gain material. However, the optical and thermal properties of InGaAs and InGaAsP are very similar. This qualifies our calculation for N-750 as a good estimation of the FTF generated in the reported device. At 77K, in comparison to the simulation result of 0.04 nm found in this study, the empirical linewidth is

TABLE III
LINEWIDTH BROADENING UNDER ROOM TEMPERATURE WITH VARYING
RADIUS OF GAIN REGION AND A FIXED OUTER RADIUS

$R_2 = 350nm$					
$R_1(nm)$	225	250	275		
$\Delta v(GHz)$	137.2	135.1	134.2		
$\Delta\lambda(nm)$	1.06	1.14	1.22		
$R_2 = 900nm$					
$R_1(nm)$	750	775	800		
$\Delta v(GHz)$	20	19.2	18.3		
$\Delta\lambda(nm)$	0.16	0.16	0.15		

0.9nm in [20]. This indicates that FTF is not a negligible noise source for nanolaser linewidth at this temperature. The discrepancy can be explained by three factors: 1) The interior temperature of the device can be much higher than the ambient temperature while being pumped. For example, [47] shows that the internal lattice temperature of a device can be 53K higher than the ambient temperature during experiment. Therefore, a broader linewidth is expected for a higher temperature. 2) Pump fluctuations also contribute to the thermal fluctuations in a nanolaser through thermal impedance [48]. 3) The empirical linewidth reported in [20] is limited by the resolution of the spectrometer. The actual linewidth, in principle, can be much smaller than 0.9nm, Therefore, it can be inferred that FTF can be a pronounced contribution to the linewidth broadening in metallo-dielectric nanolasers.

## V. CONCLUSION

In this article, we analytically and numerically investigate the linewidth broadening for a nanolaser caused by the FTF. We adopted a 2-D heat transport model to facilitate solving the stochastic thermal diffusion equation, aiming at finding the solution for the spatially and temporally dependent FTF. For better understanding the implications of the decrease of the mode volume, we derived the frequency noise for two nanolasers with different radii. We observed a higher noise floor and a larger 3-dB thermal noise modulation bandwidth for the nanolaser with smaller radius. We also deduced the thermal linewidth broadening due to FTF and arrived at 1.14nm, 0.31nm and 5.4pm for N-250 and 0.16nm, 0.04nm and 2pm for N-750, both under 300K, 77K and 4K, respectively. This observation corroborates that the ultra-small mode volume of a nanolaser could be detrimental to its spectral properties as it is more prone to fundamental thermal fluctuations. A linear dependence of linewidth broadening on the ambient temperature could be observed for both N-250 and N-750. In this manuscript, we specifically choose a metallo-dielectric nanolaser for calculation. From the comparison between two devices that have different mode volumes, it is reasonable to assume that nanolasers in general will exhibit larger finite linewidths than conventional lasers with larger mode volumes, due to the pronounced FTF in nano-resonaters.

#### APPENDIX

A. The Coefficient in the Particular Solutions for Electric Field Distribution in (3)

$$k_i = \sqrt{\left(\frac{2\pi\sqrt{\epsilon_i}}{\lambda}\right)^2 - \left(\frac{\pi}{1.1}H\right)^2}$$

where  $\epsilon_i = 11.56$  for InGaAsP, 2.14 for SiO<sub>2</sub> and 130 – 3*i* for Silver at room temperature [15]. Here, we are given the discrete value from 3-D FEM simulation, and we use E<sub>D</sub> to represent the data set. We let  $E_{D_0} = E_D/max~(E_D)$  to denote the data set that gives the normalized field distribution. R denotes the data set of the radial coordinate of all the values. We then have the normalization coefficient *n* as:

$$n = \frac{1}{\sqrt{2\pi \, \int_V r |E_{E_0}|^2 dr}}$$

Let  $E_{R_1} = E_{D_0}(R = R_1)$  and  $E_{R_2} = E_{D_0}(R = R_2)$ , we have:

$$\begin{split} A_1 &= n*max \left(J_1\left(k_1R\right)\right) \\ A_2 &= n*\frac{E_{R_2}}{J_1\left(k_2R_2\right) + B_2Y_1\left(k_2R_2\right)} \\ B_2 &= n*\frac{J_1\left(k_2R_2\right) * E_{R_1} - J_1\left(k_2R_1\right) * E_{R_2}}{Y_1\left(k_2R_1\right) * E_{R_2} - Y_1\left(k_2R_2\right) * E_{R_1}} \\ B_3 &= n*\frac{E_{R_2}}{K_1\left(k_3R_2\right)} \\ B_1 &= A_3 = 0 \end{split}$$

While for  $a_i$  and  $b_i$ :

$$a_i(orb_i) = \frac{1}{n} \frac{\max(E_D)}{\max(J_1(k_1R))} A_i(orB_i)$$

B. Calculation of PSD of the Fundamental Thermal Noise Using Langevin Approach and Green's Function Method

The stochastic thermal diffusion equation reads:

$$\frac{\partial \Delta T(\vec{r}, t)}{\partial t} - D_T \nabla_{\vec{r}}^2 \Delta T(\vec{r}, t) = F(\vec{r}, t)$$
 (B1)

The parameters here are the same as defined above. To solve the above equation, boundary conditions are needed. To start with, the silver layer is considered as an effective heat sink due to its large heat conductivity, so no thermal fluctuation happens in the metal-dielectric interface. Moreover, the temperature fluctuation and its flux need to be continuous at the boundaries.

$$\Delta T|_{R_2} = 0$$

$$\Delta T|_{R_1-0} = \Delta T|_{R_1+0}$$

$$\eta_1 \left. \frac{\partial \Delta T}{\partial r} \right|_{R_1-0} = \eta_2 \left. \frac{\partial \Delta T}{\partial r} \right|_{R_1+0}$$
(B2)

Because of the random nature of  $F(\vec{r}, t)$ , there is no first order characterization for it, but its second order characterization is known as:

$$\langle \tilde{F}(r, iw) \, \tilde{F}^* \left( r', iw' \right) \rangle$$

$$= \frac{4\pi \, D_T \, A k_B T^2}{\rho c \, V} \nabla_r \nabla_{r'} \delta \left( r - r' \right) \delta \left( w - w' \right) \quad (B3)$$

This indicates that our heat source is a point source. Since we are investigating the resonance frequency deviation contributed by the whole cavity, thermodynamic fluctuations of the temperature need to be integrated over the entire mode volume:

$$\Delta \bar{T}(t) = \int_{V} \Delta T(r, t) |E(r)|^{2} r dr$$
 (B4)

Due to the stochastic nature of the internal heat source, a Green's function method is applied to derive the analytical solution for the temperature fluctuation, and consequently, the frequency noise in the nanocavity. To analyze the spectrum, a Fourier transform is performed on (B1) and the corresponding Green's function produces:

$$iwG(\vec{r}, \vec{r}'; iw) - D_T \nabla_{\vec{r}}^2 G(\vec{r}, \vec{r}'; iw) = \delta(\vec{r} - \vec{r}')$$
 (B5)

From the definition of Green's function:

$$\Delta \tilde{T}(\vec{r}, iw) = \int_{V} G(\vec{r}, \vec{r}'; iw) \tilde{F}(\vec{r}, iw) d\vec{r}'$$
 (B6)

Given (B4) and (B6), using the Wiener-Khinchin theorem, the single-sided PSD,  $S_{\Delta T}(w)$ , of the temperature fluctuation can then be derived as:

$$S_{\Delta T}(w) = 2 \times \frac{1}{2\pi} \langle \Delta \tilde{T}(w) \Delta \tilde{T}^*(w') \rangle$$

$$= \frac{1}{\pi} \int_{V} \int_{V} |E(r)|^2 |E(r')|^2 r r' dr dr'$$

$$\times \int_{V} \int_{V} G(r, r_1; iw) G^*(r', r_2; iw')$$

$$\times \langle \tilde{F}(r_1, iw) \tilde{F}^*(r_2, iw') \rangle dr_1 dr_2 \qquad (B7)$$

According to the Van Vliet-Fassett theorem [49], the quadratic Green's function can be transformed to be linear, which gives:

$$< \Delta \tilde{T}(r, iw) \Delta \tilde{T}^*(r', iw')$$

$$\geq \frac{4\pi Ak_B T^2}{\rho c V} Re \left[ G(r, r'; iw) \right] \delta(w - w') \quad (B8)$$

And (B7) becomes:

$$S_{\Delta T}(w) = \frac{4\pi Ak_B T^2}{\rho c V} \int_{V} \int_{V} Re \left[ G\left(r, r'; iw\right) \right] \times \left| E\left(r\right) \right|^2 \left| E\left(r'\right) \right|^2 r r' dr dr' \quad (B9)$$

For a pure 2D problem we transfer (B5) into cylindrical coordinates:

(B2) 
$$\frac{d^2G\left(\vec{r},\vec{r}';iw\right)}{dr^2} + \frac{1}{r}\frac{dG\left(\vec{r},\vec{r}';iw\right)}{dr} + k^2G\left(\vec{r},\vec{r}';iw\right)$$

$$= -\frac{1}{D_TL}\delta\left(r - r'\right)\delta\left(w - w'\right) \quad (B10)$$

where  $k^2 = -iw/D_T$ . To obtain the analytical solution of the Green's function in (B10), homogeneous boundary conditions at all medium interfaces are applied. At the point heat source, the continuity of the Green's Function and the discontinuity of its derivative add two more boundary conditions, and the

latter could be derived by doing an integration of (B10) from r'-0 to r'+0:

$$G|_{r'-0} = G|_{r'+0}, r \left. \frac{\partial G}{\partial r} \right|_{r'-0}^{r'+0} = -\frac{1}{D_T L}$$

$$G|_{R_1-0} = G|_{R_1+0}, \eta_1 \left. \frac{\partial G}{\partial r} \right|_{R_1-0} = \eta_2 \left. \frac{\partial G}{\partial r} \right|_{R_1+0}$$

$$G|_{R_2} = 0 \tag{B11}$$

Solutions for Green's function in this radial symmetric problem are Bessel functions:

$$0 \leq r \leq r',$$

$$G_{1}^{<}(r, r'; iw) = g_{1}(r') J_{0}(k_{\rho 1}r)$$

$$r' < r \leq R_{1},$$

$$G_{1}^{>}(r, r'; iw) = g_{2}(r') J_{0}(k_{\rho 1}r) + h_{2}(r') H_{0}^{(1)}(k_{\rho 1}r)$$

$$R_{1} \leq r \leq R_{2},$$

$$G_{2}(r, r'; iw) = g_{3}(r') J_{0}(k_{\rho 2}r) + h_{3}(r') Y_{0}(k_{\rho 2}r)$$
(B12)

C. The Coefficients in the Particular Solutions for Green's Function in (9)

Define:

$$J_{ijk} = J_i \left( k_{\rho j} r_k \right)$$

For instance:

$$J_{011} = J_0 (k_{o1} r_1)$$

Similarly, we define  $Y_{ijk} = Y_i(k_{\rho j}r_k)$ . We also define Hankel functions as:

$$\begin{split} H_{0111} &= H_0^{(1)}(k_{\rho 1} r_1) \\ H_{1111} &= H_1^{(1)}(k_{\rho 1} r_1) \\ J_{01r} &= J_0\left(k_{\rho 1} r'\right) \\ J_{11r} &= J_0\left(k_{\rho 1} r'\right) \\ H_{011r} &= H_0^{(1)}(k_{\rho 1} r') \\ H_{111r} &= H_1^{(1)}(k_{\rho 1} r') \end{split}$$

Define a coefficient to help simplify the expressions:

$$\begin{split} &\Lambda = \frac{\eta_1 k_{\rho 1}}{\eta_2 k_{\rho 2}} \times \frac{J_{021} Y_{022} - J_{022} Y_{021}}{J_{121} Y_{022} - J_{022} Y_{121}} \\ g_1 &= \frac{g_2 J_{01r} + h_2 H_{011r}}{J_{01r}} \\ g_2 &= \frac{\Lambda H_{1111} - H_{0111}}{J_{121} - \Lambda J_{111}} h_2 \\ h_2 &= \frac{1}{D_1 H k_{\rho 1} r'} \frac{J_{01r}}{J_{01r} H_{111r} - H_{011r} J_{11r}} \\ g_3 &= \frac{\eta_1 k_{\rho 1}}{\eta_2 k_{\rho 2}} Y_{022} \times \frac{g_2 J_{111} + h_2 H_{111}}{J_{121} Y_{022} - J_{022} Y_{121}} \\ h_3 &= -\frac{J_{022}}{Y_{022}} g_3 \end{split}$$

#### REFERENCES

- [1] T. Baba, "Biosensing using photonic crystal nanolasers," MRS Commun., vol. 5, no. 4, pp. 555-564, Dec. 2015.
- [2] K. Watanabe et al., "Label-free and spectral-analysis-free detection of neuropsychiatric disease biomarkers using an ion-sensitive GaInAsP nanolaser biosensor," Biosens. Bioelectron., vol. 117, pp. 161-167,
- [3] S. Kita, Y. Nishijima, H. Misawa, and T. Baba, "Label-free biosensing utilizing ultrasmall photonic crystal nanolaser," in Proc. Adv. Opt. Sci. Congr., 2009, pp. 1-3.
- X. Wu et al., "Nanowire lasers as intracellular probes," Nanoscale, vol. 10, no. 20, pp. 9729-9735, 2018.
- M. Schubert et al., "Lasing within live cells containing intracellular optical microresonators for barcode-type cell tagging and tracking," Nano Lett., vol. 15, no. 8, pp. 5647-5652, Jul. 2015.
- A. H. Fikouras et al., "Non-obstructive intracellular nanolasers," Nat. Commun., vol. 9, no. 1, p. 4817, Nov. 2018.
- R.-M. Ma and R. F. Oulton, "Applications of nanolasers," Nature Nanotechnol., vol. 14, no. 1, pp. 12-22, 2019.
- M. Lorke, T. Suhr, N. Gregersen, and J. Mørk, "Theory of nanolaser devices: Rate equation analysis versus microscopic theory," Phys. Rev. B Condens. Matter Mater. Phys., vol. 87, no. 20, pp. 1-10, May 2013.
- [9] T. Suhr, N. Gregersen, K. Yvind, and J. Mørk, "Modulation response of nanoLEDs and nanolasers exploiting Purcell enhanced spontaneous emission," Opt. Exp., vol. 18, no. 11, 2010, Art. no. 11230.
- Q. Gu et al., "Purcell effect in sub-wavelength semiconductor lasers," Opt. Express, vol. 21, no. 13, 2013, Art. no. 15603.
- [11] S. Kedia, "Laser emission from self-assembled active photonic crystal matrix," J. Nanophotonics, vol. 4, no. 1, 2010, Art. no. 049506.
- [12] K. Xu, "Integrated silicon directly modulated light source using p-well in standard CMOS technology," IEEE Sensors J., vol. 16, no. 16, pp. 6184-6191, Aug. 2016.
- T. C. Chui, D. R. Swanson, M. J. Adriaans, J. A. Nissen, and J. A. Lipa, "Temperature fluctuations in the canonical ensemble," Phys. Rev. Lett., vol. 69, no. 21, pp. 3005-3008, Nov. 1992.
- [14] L. D. Landau and E. M. Lifshitz, Course of Theoretical Physics, vol. 5, Oxford, U.K: Pergamon Press. 1980.
- [15] M. P. Nezhad et al., "Room-temperature subwavelength metallodielectric lasers," Nature Photon., vol. 4, pp. 395-399, Apr. 2010.
- M. Khajavikhan et al., "Thresholdless nanoscale coaxial lasers," Nature, vol. 482, pp. 204-207, Feb. 2012.
- [17] B. Ellis et al., "Ultralow-threshold electrically pumped quantum-dot photonic-crystal nanocavity laser," Nature Photon., vol. 5, pp. 297-300,
- [18] D. Saxena et al., "Optically pumped room-temperature GaAs nanowire lasers," Nature Photon., vol. 7, no. 12, pp. 963-968, Dec. 2013.
- [19] K. Ding and C. Z. Ning, "Metallic subwavelength-cavity semiconductor nanolasers," Light Sci. Appl., vol. 1, pp. 1-8, Jul. 2012.
- [20] J. H. Lee et al., "Electrically pumped sub-wavelength metallo-dielectric pedestal pillar lasers," Opt. Express, vol. 19, no. 22, 2011,
- [21] K. Ding, M. T. Hill, Z. C. Liu, L. J. Yin, P. J. V. Veldhoven, and C. Z. Ning, "Record performance of electrical injection sub-wavelength metallic-cavity semiconductor lasers at room temperature," Opt. Express, vol. 21, no. 4, 2013, Art. no. 4728.
- [22] S. H. Pan, Q. Gu, A. E. Amili, F. Vallini, and Y. Fainman, "Dynamic hysteresis in a coherent high-ß nanolaser," *Optica*, vol. 3, no. 11, p. 1260,
- Y.-J. Lu et al., "Plasmonic nanolaser using epitaxially grown silver film," Science, vol. 337, no. 6093, pp. 450-453, Jul. 2012.
- [24] M. T. Hill et al., "Lasing in metallic-coated nanocavities," Nature Photon., vol. 1, pp. 589-594, Sep. 2007.
- [25] M. A. Noginov et al., "Demonstration of a spaser-based nanolaser," Nature, vol. 460, pp. 1110-1112, Aug. 2009.
- [26] H. Altug, D. Englund, and J. Vučković, "Ultrafast photonic crystal
- nanocavity laser," *Nature Phys.*, vol. 2, pp. 484–488, Jul. 2006. H.-G. Park *et al.*, "Electrically driven single-cell photonic crystal laser," Science, vol. 305, no. 5689, pp. 1444-1447, 2004.
- [28] K. Kikuchi, "Fundamentals of coherent optical fiber communications," J. Lightw. Technol., vol. 34, no. 1, pp. 157-179, Jun. 1, 2016.
- [29] S. S. Harilal, N. L. Lahaye, and M. C. Phillips, "High-resolution spectroscopy of laser ablation plumes using laser-induced fluorescence," Opt. Express, vol. 25, no. 3, p. 2312, Feb. 2017.
- [30] S. Foster, A. Tikhomirov, and M. Milnes, "Fundamental thermal noise in distributed feedback fiber lasers," IEEE J. Quantum Electron., vol. 43, no. 5, pp. 378-384, May 2007.

- [31] H. Meštrić, R.-A. Eichel, K.-P. Dinse, A. Ozarowski, J. V. Tol, and L. C. Brunel, "High-frequency electron paramagnetic resonance investigation of the Fe<sup>3+</sup> impurity center in polycrystalline PbTiO<sub>3</sub> in its ferroelectric phase," *J. Appl. Phys.*, vol. 96, no. 12, pp. 7440–7444, 2004.
- [32] G. E. Shtengel, R. F. Kazarinov, G. L. Belenky, M. S. Hybertsen, and D. A. Ackerman, "Advances in measurements of physical parameters of semiconductor lasers," *Int. J. High Speed Electron. Syst.*, vol. 9, no. 4, pp. 901–940, Dec. 2000.
- [33] S. S. Deka, S. H. Pan, Q. Gu, Y. Fainman, and A. E. Amili, "Coupling in a dual metallo-dielectric nanolaser system," *Opt. Lett.*, vol. 42, no. 22, pp. 4760–4763, Nov. 2017.
- [34] A. Mizrahi, V. Lomakin, B. A. Slutsky, M. P. Nezhad, L. Feng, and Y. Fainman, "Low threshold gain metal coated laser nanoresonators," *Opt. Lett.*, vol. 33, no. 11, pp. 1261–1263, 2008.
- [35] C.-Y. Fang, F. Vallini, A. El Amili, J. S. T. Smalley, and Y. Fainman, "Low resistance tunnel junctions for efficient electrically pumped nanolasers," *IEEE J. Sel. Topics Quantum Electron.*, vol. 23, no. 6, Dec. 2017, Art. no. 1500506.
- [36] K. Xu, "Silicon MOS optoelectronic micro-nano structure Based on reverse-biased PN junction," *Phys. Status Solidi*, vol. 216, no. 7, Mar. 2019, Art. no. 1970029.
- [37] V. B. Braginsky, M. L. Gorodetsky, and S. Vyatchanin, "Thermodynamical fluctuations and photo-thermal shot noise in gravitational wave antennae," *Phys. Lett. A*, vol. 264, no. 1, pp. 1–10, Dec. 1999.
- [38] M. L. Gorodetsky and I. S. Grudinin, "Fundamental thermal fluctuations in microspheres," J. Opt. Soc. Amer. B, vol. 21, no. 4, p. 697, 2004.
- [39] T. Liu and Q. J. Wang, "Fundamental frequency noise and linewidth broadening caused by intrinsic temperature fluctuations in quantum cascade lasers," *Phys. Rev. B, Condens. Matter*, vol. 84, no. 12, Sep. 2011, Art. no. 125322.
- [40] K. M. Van Vliet and E. R. Chenette, "Noise spectra resulting from diffusion processes in a cylindrical geometry," *Physica*, vol. 31, no. 7, pp. 985–1001, Jul. 1965.
- [41] K. M. V. Vliet and H. Mehta, "Theory of transport noise in semiconductors," *Phys. Status Solidi*, vol. 106, no. 1, pp. 11–30, 1981.
- [42] L. A. Coldren, S. W. Corzine, and M. Mashanovitch, *Diode Lasers and Photonic Integrated Circuits*. Hoboken, NJ, USA: Wiley, 2012, pp. 303-308
- [43] K. Petermann, Laser Diode Modulation and Noise. Dordrecht, The Netherlands: Kluwer, 1991.pp. 196–198.
- [44] K. Ding, L. Yin, M. T. Hill, Z. Liu, P. J. V. Veldhoven, and C. Z. Ning, "An electrical injection metallic cavity nanolaser with azimuthal polarization," *Appl. Phys. Lett.*, vol. 102, no. 4, 2013, Art. no. 041110.
- [45] K. Ding et al., "CW operation of a subwavelength metal-semiconductor nanolaser at record high temperature under electrical injection," in Proc. IEEE Winter Topicals, Jan. 2011, pp. 15–16.
- [46] C.-Y. Fang et al., "Lasing action in low resistance nanolasers based on tunnel junctions," Opt. Lett., vol. 44, no. 15, pp. 3669–3672, 2019.
- [47] Q. Gu, J. S. Smalley, J. Shane, O. Bondarenko, and Y. Fainman, "Temperature effects in metal-clad semiconductor nanolasers," *Nanophotonics*, vol. 4, no. 1, pp. 26–43, 2015.
- [48] S. De, "Noise in dual-frequency semiconductor and solid-state lasers," Ph.D. dissertation, Dept. Phys., Univ. Paris-Sud, Orsay, France, 2015.
- [49] R. E. Burgess, Fluctuation Phenomena in Solids. New York, NY, USA: Academic, 1969, p. 267.



Si Hui Pan received the B.S. degree in physics from Brandeis University, Waltham, MA, USA, in 2010, and the M.S. degree in physics from the University of California at San Diego, La Jolla, CA, USA, in 2013, where she is currently pursuing the Ph.D. degree. Her research interests include the fabrication and characterization of nanophotonic devices, solid-state physics, and quantum optics. Especially, she is investigating the coherent and dynamical properties of metal-clad nanolasers based on InGaAsP multiple quantum wells.

Prior to graduate school, she held a research staff position for two years at the Massachusetts Institute of Technology Lincoln Laboratory, Lexington, MA, USA, where she participated in the research and development of superconducting nanowire single photon detectors. She has held undergraduate research positions at the Daghlian Ion Accelerator Lab, Connecticut College; the Laboratory for Elementary Particle Physics, Cornell University; and the National Nanotechnology Infrastructure Network, Harvard University, where she investigated the optical properties of silicon supersaturated with chalcogens for her undergraduate honors thesis. Upon receiving the B.S. degree, she received a research internship position at the National Institute for Material Science, Tsukuba, Ibaraki, Japan.

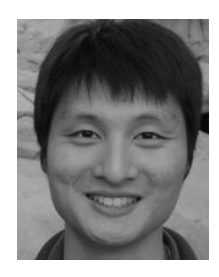
Ms. Pan was a recipient of the National Science Foundation Graduate Research Fellowship, the Physics Excellence Award from University of California at San Diego, and the Physics Faculty Prize from Brandeis University.



**Suruj S. Deka** received the B.E. (magna cum laude) and the M.S degrees in electrical engineering from Vanderbilt University in Nashville, Tennessee, in 2015, as a part of an accelerated 4-year-dual-degree program. He is currently pursuing the Ph.D. degree in electrical engineering (nanoscale devices and systems) with the University of California at San Diego. His master's thesis at Vanderbilt University was Memristance Phenomenon in TiO2-Porous Silicon Nanocomposites and involved material and electrical characterization of memristive devices. His

main research interest concerns modeling, fabrication and characterization of III-V nanolaser devices.

Mr. Deka was a recipient of the Jacobs Fellowship from 2015 to 2016 and the Sandstrom Fellowship from 2016 to 2017.



Cheng-Yi Fang received the B.S. and M.S. degrees from National Taiwan University, Taipei, Taiwan. He is currently pursuing the Ph.D. degree with the Ultrafast and Nanoscale Optics Group, University of California at San Diego, San Diego, San Diego, CA, USA. His research interests include photonics, semiconductor lasers, and plasmonics.



Sizhu Jiang received the B.E. degree in electrical engineering from the Peking University of Posts and Telecommunication, Beijing, China, in 2017, with research background in Fiber Bragg Grating sensors and wearable medical device, the M.S. degree in electrical engineering from the University of California at San Diego, San Diego, CA, USA, in 2019, where he is currently pursuing the Ph.D. degree an emphasis on photonics. Her research interests include design, fabrication, and characterization of nanoscale photonic devices, dynamics of

nanoscale lasers, coupled resonators, and optical phased arrays.



Zijun Chen received the B.S. degree in electrical engineering from the University of California at San Diego, La Jolla, CA, USA, in 2018, where he is currently pursuing the M.S. degree in electrical engineering with an emphasis on photonics as part of a contiguous B.S./M.S. program for advanced undergraduates. His research interests include on-chip III-V semiconductor laser, Si compatible integrated optics, and integrated quantum optics.



Yeshaiahu (Shaya) Fainman received the M.Sc. and Ph.D. degrees from Technion in 1979 and 1983, respectively. He is currently an inaugural Cymer Chair Professor of advanced optical technologies and a Distinguished Professor in electrical and computer engineering (ECE) with the University of California at San Diego (UCSD), San Diego. He is directing research of the Ultrafast and Nanoscale Optics Group, UCSD, and made significant contributions to near field optical phenomena, inhomogeneous and meta-materials, nanophotonics and plasmonics, and

non-conventional imaging.

He contributed more than 280 manuscripts in peer review journals and more than 450 conference presentations and conference proceedings. His current research interests are in near field optical science and technology with applications to information technologies and biomedical sensing. He is a fellow of the Optical Society of America and the Society of Photo-Optical Instrumentation Engineers. He was a recipient of the Miriam and Aharon Gutvirt Prize, the Lady Davis Fellowship, the Brown Award, the Gabor Award, the Emmett N. Leith Medal, and the Joseph Fraunhofer Award/Robert M. Burley Prize.



Abdelkrim El Amili received the B.Sc. degree in physics and engineering and the M.Sc. degree in fundamental physics from the University of Bordeaux 1, Talence, France, in 2004 and 2006, respectively, and the Ph.D. degree in physics from the University of Paris-Sud XI, Orsay, France, in 2010. His thesis work was on the realization of an experimental setup for atom detection in atom-chips, and on the theoretical investigation of detection performances of coupled micro-cavities.

From 2010 to 2011, he was a Post-Doctoral Researcher in laser physics with the Laboratoire Aimé Cotton, Paris. From 2011 to 2014, he was a Non-Permanent Researcher with the Institut de Physique de Rennes 1, CNRS-University of Rennes 1. In 2015, he joined the ECE Department, University of California at San Diego (UC San Diego), where he is currently a Research Scientist. His research was on the experimental and theoretical study of the dynamics of solid-state lasers. Particularly, he focused on the development of optical methods enabling strong suppressions of inherent resonant intensity noises in single-/dual-frequency solid-state lasers. His research interests lie in both III-V and Silicon nanophotonics.